図1 一般的なアルキルグルコシド

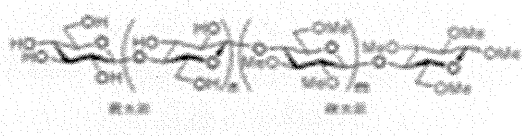

図2 新規に開発したメチルセルロース系ノニオン性界面活性剤

骨格の全てがセルロースの部分構造からなっています。

それではこの新しいノニオン性界面活性剤にはどのような性質があるのでしょうか。最近、その界面活性能は既存のアルキルグリコシドと同等ですが、細胞毒性はアルキルグリコシドより低いことがわかりました。アルキルグリコシドは細胞膜中に存在する膜タンパク質を取り出す際に利用されています。つまり、アルキルグリコシドは細胞膜の脂質二重層を破壊しているわけですが、この状況は生きた細胞にとっては死を意味します。

これに対し、この新規ノニオン性界面活性剤はアルキルグリコシドと同等の界面活性能を有しつつ、より人体や環境に優しいという性質を備えています。もっとも、細胞毒性が低い理由については未だ明らかにされていません。そのため、その「なぜ？」を明らかにする更なる研究成果が期待されています。

※注　PRTR制度とは、人の健康や生態系に有害な恐れのある化学物質について、事業所からの環境（大気、水、土壌）への排出量および廃棄物に含まれている化合物の、事業所外への移動量を事業者自らが把握し国に対して届け出るとともに国は届け出データや推計に基づき、排出量・移動量を集計し公表する制度です。

（京都大学　上高原 浩）

NEUROPATHOLOGY

Neuropathology 2012; **32**, 124–132 doi:10.1111/j.1440-1789.2011.01245.x

Original Article

Protease-resistant PrP and PrP oligomers in the brain in human prion diseases after intraventricular pentosan polysulfate infusion

Hiroyuki Honda,[1] Kensuke Sasaki,[1] Haruhiko Minaki,[1] Kenta Masui,[1] Satoshi O. Suzuki,[1] Katsumi Doh-ura[2] and Toru Iwaki[1]

[1]Department of Neuropathology, Graduate School of Medical Sciences, Kyushu University, Fukuoka and [2]Department of Neurochemistry, Tohoku University Graduate School of Medicine, Sendai, Japan.

Intraventricular infusion of pentosan polysulfate (PPS) as a treatment for various human prion diseases has been applied in Japan. To evaluate the influence of PPS treatment we performed pathological examination and biochemical analyses of PrP molecules in autopsied brains treated with PPS (one case of sporadic Creutzfeldt-Jakob disease (sCJD, case 1), two cases of dura mater graft-associated CJD (dCJD, cases 2 and 4), and one case of Gerstmann-Sträussler-Scheinker disease (GSS, case 3). Six cases of sCJD without PPS treatment were examined for comparison. Protease-resistant PrP (PrP^{res}) in the frontal lobe was evaluated by Western blotting after proteinase K digestion. Further, the degree of polymerization of PrP molecules was examined by the size-exclusion gel chromatography assay. PPS infusions were started 3–10 months after disease onset, but the treatment did not achieve any clinical improvements. Postmortem examinations of the treated cases revealed symmetrical brain lesions, including neuronal loss, spongiform change and gliosis. Noteworthy was GFAP in the cortical astrocytes reduced in all treated cases despite astrogliosis. Immunohistochemistry for PrP revealed abnormal synaptic deposits in all treated cases and further plaque-type PrP deposition in case 3 of GSS and case 4 of dCJD. Western blotting showed relatively low ratios of PrP^{res} in case 2 of dCJD and case 3 of GSS, while in the treated sCJD (case 1), the ratio of PrP^{res} was comparable with untreated cases. The indices of oligomeric PrP were reduced in one sCJD (case 1) and one dCJD (case 2). Although intraventricular PPS infusion might modify the accumulation of PrP oligomers in the brains of patients with prion diseases, the therapeutic effects are still uncertain.

Key words: Creutzfeldt-Jakob disease, oligomer, pentosan polysulfate, prion protein, size-exclusion gel chromatography.

INTRODUCTION

Prion diseases, also known as transmissible spongiform encephalopathies (TSEs), are fatal neurodegenerative disorders that include Creutzfeldt-Jakob disease (CJD) and Gerstmann-Sträussler-Scheinker disease (GSS) in humans, and scrapie and bovine spongiform encephalopathy in animals. In these diseases, histopathological changes in the brain are characterized by spongiform change, reactive changes of astrocytes and variable loss of neurons.[1] In addition, deposition of a protease-resistant isoform of prion protein (PrP^{res}) is detected in the brain. This PrP^{res} contains high β-sheet content and is composed of polymerized PrP molecules post-translationally converted from normal, cellular PrP (PrP^{c}) of 254-amino acid 32–35 kDa glycolipid-anchored, plasma membrane protein that is widely expressed in the CNS.[2]

There is currently no effective remedy for human prion diseases, but several therapeutic compounds including quinacrine and pentosan polysulfate (PPS) have been tested for patients with prion diseases on experimental trial bases. Quinacrine is reportedly effective in inhibiting PrP^{res} formation in prion-infected cells.[3,4] However, subsequent studies showed no apparent beneficial effects of quinacrine in either experimental animals or humans.[5–7] By comparison, PPS has been shown to prevent the propagation of

Correspondence: Hiroyuki Honda, MD, Department of Neuropathology, Graduate School of Medical Sciences, Kyushu University, 3-1-1 Maidashi, Higashi-ku, Fukuoka 812-8582, Japan. Email: h-hiroyu@np.med.kyushu-u.ac.jp

Received 28 May 2011; revised 23 June 2011 and; accepted 25 June 2011; published online 1 August 2011.

PrP^{res} in prion-infected cells.[8] Additionally, in experimental animals PPS has been administered directly into the CNS via an intra-hemiventricular canula, resulting in significant prolongation of the incubation periods accompanied with the laterality of neuropathological changes.[9] PPS inhibits PrP^{res} formation by interfering with the interaction of PrP^{c} and PrP^{res} with endogenous glycosaminoglycan or proteoglycan.[10] In addition, PPS stimulates endocytosis of PrP^{c}, reducing the amount of PrP^{c} present on the cell surface.[11] Experimental trials of intraventricular PPS infusion in the patients with prion diseases have been performed on observational bases, and thus it has been difficult to prove its efficacy.[12,13] In fact, Tsuboi *et al.* reported that PPS treatment showed no apparent improvements of clinical features in Japanese patients with prion disease.[14] In comparison, Bone *et al.* reported that mean survival of seven patients with PPS treatment was longer than reported values for the natural history of prion diseases in the United Kingdom, although possible reasons for this finding remain unclear.[15]

The main pathogenic component in prion diseases has been suggested to be PrP^{res} composed of PrP polymers. Recently, PrP oligomers, equivalent to 14–28 PrP molecules were reported as the most infectious units.[16,17] In addition, Kristiansen *et al.* reported that disease-associated PrP oligomers inhibit the 26S proteasome and cause neurotoxicity.[18] We have previously developed a gel-filtration chromatography method using spin columns to examine PrP oligomers, and revealed that increased PrP oligomers correlated with the degree of histopathological changes such as spongiform change and gliosis.[19] In other neurodegenerative diseases, including Alzheimer's disease, dementia with Lewy bodies and Parkinson's disease, soluble oligomers of amyloidogenic proteins were proposed to be the principal neurotoxic agents.[20,21]

In this report, to clarify the influence of PPS treatment on brains affected with piron diseases, we performed pathological examination and biochemical analyses of PrP, including its degree of polymerization, in four cases of prion diseases treated with PPS.

MATERIALS AND METHODS

We investigated the degree of polymerization of PrP molecules in four prion diseases cases that received PPS treatment, denoted PPS(+): one case of sporadic CJD (sCJD), two cases of dura mater graft-associated CJD (dCJD), and one case of GSS. We also examined six cases of sCJD without PPS treatment, denoted PPS(–), for comparison. The profiles of the patients are summarized in Table 1. At autopsy the brains were weighed and fixed with 10% buffered formalin. Six micrometer-thick sections of paraffin-embedded tissue from the CNS were stained with HE and the KB staining method. Immunohistochemistry was performed with primary antibodies against anti-prion antibody (mouse monoclonal 3F4, 1:400; Signet, Dedham, MA, USA) and GFAP (rabbit polyclonal, 1:1000; Dako, Glostrup, Denmark). The sections were then treated with appropriate biotinylated secondary antibodies and the reaction products were detected using the avidin-biotinylated peroxidase complex method (ABC; Vector Laboratories, Burlingame, CA, USA) coupled with a diaminobenzidine (Dojindo, Kumamoto, Japan) reaction.

Brain homogenate preparation

Human brains were collected at autopsy from four prion disease cases that had received PPS treatment and six cases of sCJD that had not received PPS treatment. Samples of frontal cortex were frozen fresh and stored at –80°C until used. The brain samples were homogenized to a final concentration of 10% in lysis buffer with sodium dodecyl sulfate (SDS) (100 mM Tris-HCl, 100 mM NaCl, 10 mM EDTA, 1% SDS, pH 7.6) for the size-exclusion gel chromatography assay. Most PrP^{c} could be solubilized as monomers in lysis buffer with SDS.[19] Samples were homogenized

Table 1 Summary of patient profiles

Case	Diagnosis	Genotype/PrP^{res} type	Age at death	Sex	Duration of illness (months)	Duration of PPS treatment (months)	Brain weight (g)
1	sCJD	129MM/type 1	74	F	23	20	660
2	dCJD	129MM/type 1	67	M	12	9	950
3	GSS	P102L/8 kDa	70	F	20	14	1055
4	dCJD	129MM/type 1	55	M	14	4	1460
5	sCJD	129MM/type 1	71	M	10	–	562
6	sCJD	129MM/type 1	61	M	30	–	745
7	sCJD	129MM/type 1	69	M	15	–	940
8	sCJD	129MM/type 1	73	F	4	–	1100
9	sCJD	129MM/type 1	68	F	2	–	1260
10	sCJD	NA/type 1	66	M	2.5	–	1435

dCJD, dura CJD; F, female; GSS, Gerstmann-Sträussler-Scheinker disease; M, male; MM, methionine homozygote at prion protein gene codon 129; NA, not available; PPS, pentosan polysulfate; PrP^{res}, proteinase resistant isoform of prion protein; sCJD, sporadic CJD.

at 5000 rpm for 30 s in a bead disrupter homogenizing system (MicroSmash MS-100; Tomy Seiko Co., Ltd, Tokyo, Japan). Homogenates were then clarified by centrifugation at 250 *g* for 5 min and the supernatant was stored at –80°C.

Detection of PrP^{res}

Conventional procedure for the detection of PrP^{res} was conducted as follows: 1% brain homogenate was prepared in extraction buffer (100 mM Tris-HCl, 100 mmol NaCl, 10 mmol EDTA, 0.5% Nonidet P-40, 0.5% sodium deoxycholate, pH 7.6) and incubated with 50 μg/mL proteinase K (PK) at 37°C for 1 h. Protease activity was then abolished by the addition of 1 mmol Pefabloc SC (Roche, Indianapolis, IN, USA). Undigested PrP^{res} fragments were separated by SDS-PAGE in 12% NuPAGE Bis-Tris gels (Invitrogen, Carlsbad, CA, USA) and transferred onto polyvinylidene difluoride membranes (Immobilon-P; Millipore, Billerica, MA, USA). PrP was detected using anti-PrP antibody (mouse monoclonal 3F4, 1:10 000) as the primary antibody and peroxidase-conjugated anti-mouse IgG as the secondary antibody (AP192P, 1:20 000; Chemicon, Temecula, CA, USA). The immunoreaction was visualized using the ECL plus Western Blotting Detection System (GE Healthcare; Chalfont St. Giles, Buckinghamshire, UK).

Size-exclusion gel chromatography assay

We performed the size-exclusion gel chromatography assay using the spin-column kit CHROMA SPIN-200 (Clontech, San Francisco, CA, USA) that clearly separated oligomeric PrP from monomeric PrP.[19,22] The samples were first centrifuged at 120 *g* for 2 min, and the first fraction was collected in the collection tube. Another 40 μL of lysis buffer was added, and the samples were centrifuged at 120 *g* for 2 min to collect the size-exclusion fractions sequentially. In these operations, we used a centrifuge with a swing-bucket rotor (A-4–62; Eppendorf, Hamburg, Germany). Fractionated PrP was detected without PK treatment by SDS-PAGE and Western blot analysis, as described above.

RESULTS

Case reports and brain pathology

Details of PPS treatment and clinical findings from the patients were described in a previous paper.[14] In all four PPS-treated cases, the PPS infusion catheter was inserted into the right lateral ventricle, and the PPS dose was gradually escalated to the target dosage of 120 μg/kg/day. PPS treatment showed no apparent improvement of clinical features in all the cases. Clinicopathological findings from each case that had received PPS treatment are described below.

Case 1

A 72-year-old woman showed truncal ataxia and progressive gait disturbance. She had no family history of prion or neurological disease. Diffusion weighted imaging (DWI) demonstrated diffuse bilateral high-intensity signals in the cerebral cortex and striatum. Periodic synchronous discharge was seen in electroencephalography 2 months after disease onset. She was diagnosed with sCJD. Myoclonus and startle reaction were observed 3 months after the onset. The PPS infusion was started 3 months after the onset; however, no improvement in clinical features was observed. She developed akinetic mutism 6 months after the onset. Tonic seizures in extremities were also seen. The patient died of pneumonia and autopsy was performed 14.5 h after death. The brain weighed 660 g and showed severe atrophy with bilateral subdural hematoma and fluid collection. Microscopy demonstrated severe neuronal loss, rarefaction of neuropil, and gliosis across the cerebral cortices (Fig. 1A). Although astrocytosis was noted in HE staining, GFAP expression was weak in the cerebral cortices, except in subpial astrocytes (Fig. 2A). These pathological changes were also seen in the basal ganglia and thalamus. Synaptic PrP deposition was detected in the cerebral cortices, basal ganglia and thalamus (Fig. 1B). There was no laterality of spongiform change, neuronal loss, gliosis or PrP deposition.

Case 2

A 66-year-old man showed dysarthria 25 years after dura mater graft implantation because of cerebral hemorrhage. He manifested right hand clumsiness and progressive gait disturbance. Myoclonus was also seen in the right extremities. He had no family history of prion disease or neurological disease. DWI showed abnormal high-intensity signals in bilateral temporal cortices. In addition, brain biopsy was performed and revealed a type 1 PrP^{res} accumulation. The patient was diagnosed with dCJD. The electroencephalogram showed no periodic synchronous discharges. He developed akinetic mutism 2 months after disease onset. PPS infusion was started 3 months after the onset, but no improvement of clinical features was observed. The patient died of pneumonia and autopsy was performed 9 h after death. The brain weighed 950 g and showed severe atrophy with bilateral subdural fluid collection. Spongiform change, severe neuronal loss and gliosis were seen in the cerebral cortices (Fig. 1C). Astrocytosis was found in all layers of the cerebral cortex; however GFAP expression was weak (Fig. 2B). Synaptic PrP

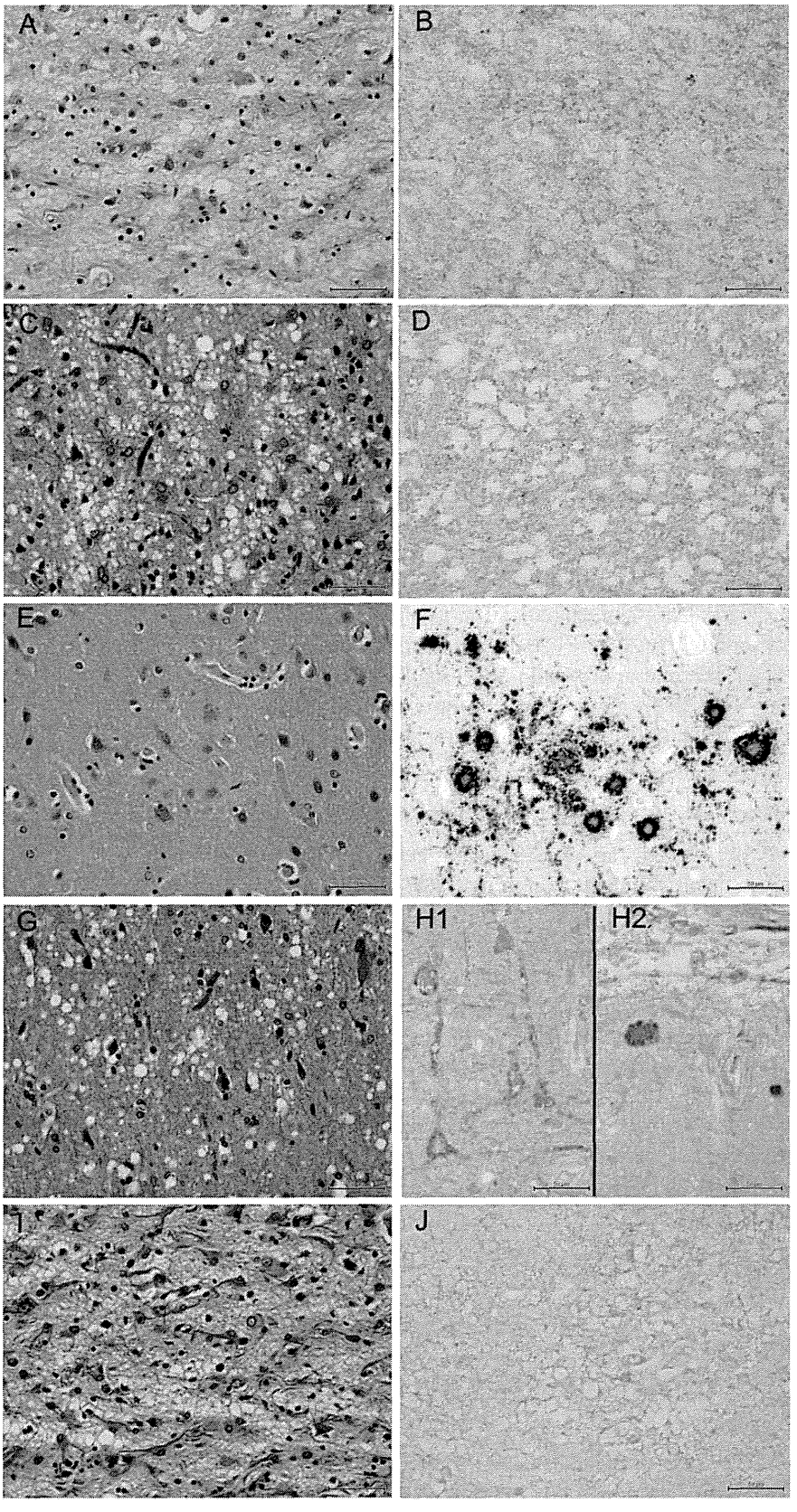

Fig. 1 Light micrographs of frontal cortices in prion diseases. A, C, E, G, I: HE stain. B, D, F, H1, H2, J: immunohistochemistry for PrP. Case 1 shows severe neuronal loss and significant rarefaction of neuropil (A) and synaptic PrP deposition (B). Case 2 shows typical spongiform change (C) and synaptic PrP deposition (D). Case 3 shows several amyloid plaques, neuronal loss and gliosis; however spongiform change is very mild (E). Both plaque-type deposition and synaptic deposition of PrP are detected (F). Case 4 shows neuronal atrophy and spongiform change (G). Synaptic deposition of PrP is mainly seen around pyramidal neurons of the deep cortical layer (H1) and plaque-type depositions are mainly found in the subpial layer (H2). Case 5 without pentosan polysulfate (PPS) treatment shows severe neuronal loss and remarkable rarefaction (I) and synaptic PrP deposition (J).

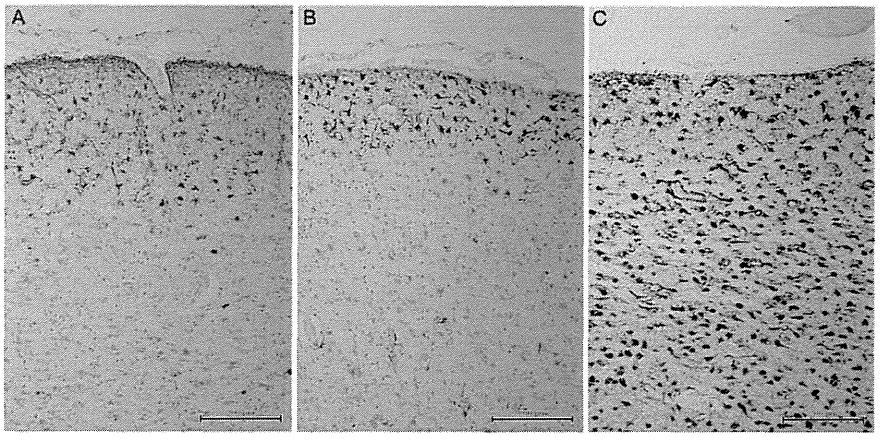

Fig. 2 Immunohistochemistry for GFAP of the frontal cortices. In case 1 (A) and case 2 (B) with pentosan polysulfate (PPS) treatment, subpial astrocytes show strong immunoreactivity for GFAP, but most cortical astrocytes show negative or weak immunoreactivity for GFAP despite their reactive morphology. In comparison, cortical astrocytes in all layers show strong GFAP immunoreactivity in case 5, which did not receive PPS treatment (C).

deposition was also detected in the cerebral cortices (Fig. 1D). No plaque-type deposition of PrP was noted. There was no laterality of spongiform change, neuronal loss, gliosis or PrP deposition.

Case 3

A 68-year-old woman showed progressive gait disturbance and dysarthria. Upper limb ataxia was also observed 5 months after disease onset. DWI showed no apparent intensity changes. The electroencephalogram showed no periodic synchronous discharges. She had a family history of prion disease. Analysis of the PrP gene revealed a P102 L mutation. She was diagnosed with GSS and the PPS infusion was started 6 months after the onset. No clinical improvement was observed. The patient died of pneumonia and autopsy was performed 27 h after death. The brain weighed 1055 g and showed moderate atrophy with bilateral subdural fluid collection. Spongiform change and neuronal loss were mild (Fig. 1E). Although astrocytosis was found in all layers of the cerebral cortices, GFAP immunoreactivity was seen mainly in the superficial cortical layers. Numerous plaque-type PrP depositions were noted in all layers of the cerebral cortices (Fig. 1F), the basal ganglia, thalamus and cerebellar granular layer. Synaptic PrP deposition was also seen in the molecular layer of the cerebral cortices, basal ganglia and thalamus. No laterality of pathological change was seen.

Case 4

A 55-year-old man showed dizziness 19 years after dura mater graft implantation. He developed dysarthria, memory deficits and character changes 8 months after disease onset. Myoclonus and startle reaction were also observed 10 months after the onset. The electroencephalogram showed no periodic synchronous discharges. DWI demonstrated high-intensity signals in the right caudate nucleus and the right thalamus. He had no family history of prion disease or neurological disease. Brain biopsy was performed and showed a type 1 PrP^{res} accumulation. The patient was diagnosed with dCJD. Although PPS infusion was started 10 months after the onset, no clinical improvement was observed. The patient died of pneumonia and autopsy was performed 13 h after death. The brain weighed 1460 g. Right subdural hematoma was noted, but brain atrophy was not apparent. Spongiform change, severe neuronal loss and gliosis were apparent in the precentral gyrus, entorhinal cortex, anterior cingulate gyrus, thalamus and putamen (Fig. 1G). Even in regions where astrocytosis was found in all layers, GFAP immunoreactivity was seen exclusively in the superficial layer of the cerebral cortices. Both synaptic deposition of PrP (Fig. 1H1) and plaque-type deposition of PrP (Figs 1,2) were noted in the cerebral cortices, basal ganglia and hippocampus. There was no laterality of spongiform change, neuronal loss, gliosis or PrP deposition.

In PPS(–) cases, HE staining revealed that the levels of neuronal loss, spongiosis and gliosis advanced in accordance with the loss of brain weight. Various levels of synaptic PrP deposition were noted in each case. In case 5, which showed severe brain atrophy, neuronal loss and rarefaction of neuropils were evident (Fig. 1I). Both astrocytosis and marked GFAP immunoreactivity were noted in all layers of the cerebral cortices (Fig. 2C). Synaptic PrP deposition was also detected in cerebral cortices (Fig. 1J).

The ratio of PrP^{res}/total PrP

Western blot analysis detected PrP^{res} and total PrP. Cases 1 and 2 showed a type 1 pattern (Fig. 3A,B). Case 3 showed PrP^{res} fragments with molecular masses of around 8 kDa (Fig. 3C). Case 4 showed PrP^{res} fragments with intermediate size between types 1 and 2 (Fig. 3D). We calculated the ratio of PrP^{res}/total PrP based on the signal intensities of the immunoblots. In PPS(–) cases, the ratio of PrP^{res}/total PrP was already increased in case 9 with mild brain

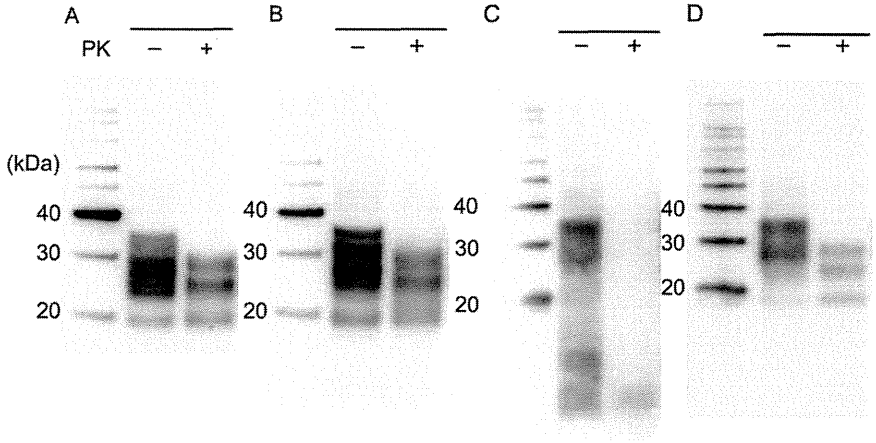

Fig. 3 Western blot analysis for PrP with or without proteinase K (PK) treatment. The brain homogenates from frontal cortices of pentosan polysulfate positive (PPS(+)) cases were separated by SDS-PAGE and probed with anti-PrP antibody (clone 3F4). The blot shows a type 1 pattern of PrP^{res} in case 1 (A) and case 2 (B). Case 3 shows PrP^{res} fragments with molecular masses of around 8 kDa (C). Case 4 shows PrP^{res} fragments with intermediate size between types 1 and 2 (D).

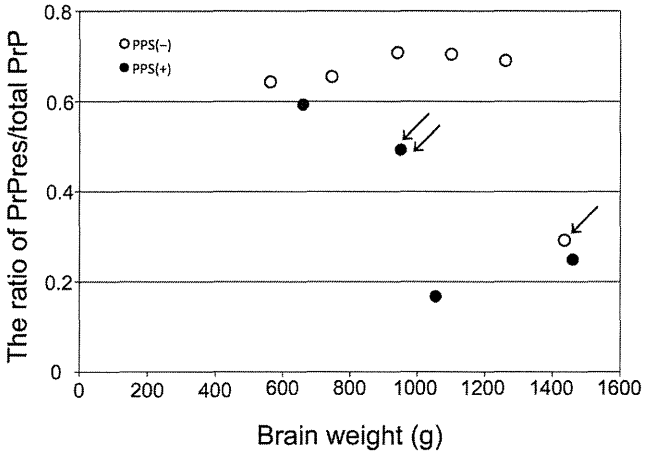

Fig. 4 Relationship between PrP^{res}/total PrP ratio and brain weight. The ratios of PrP^{res}/total PrP are markedly increased in all pentosan polysulfate negative (PPS(–)) cases (open circles) except for case 10 (arrow). Among PPS(+) cases (closed circles), case 2 (double arrows) shows a relatively low ratio of PrP^{res}/total PrP in comparison to PPS(–) cases.

atrophy. Case 2, one of three CJD cases with PPS(+), showed a relatively low ratio of PrP^{res}/total PrP in comparison to PPS(–) cases (Fig. 4).

The indices of oligomeric PrP/total PrP and monomeric PrP/total PrP

The first fraction consisted mostly of the void volume and contained insufficient protein to be assessed. Pre-column samples were taken as loading samples of total PrP. The aggregated forms of PrP were detected in fractions 2–4 (Fig. 5). Fraction 3 in this method represented the oligomeric PrP.[19,22] Thus, the index of oligomeric PrP/total PrP was obtained by dividing the intensity of fraction 3 by the intensity of the pre-column sample. Proteins with molecular weights of approximately 30 kDa, such as monomer PrP molecules, were collected mainly in fractions 6–8.[19,22] Fraction 7 represented the monomeric PrP. The index of monomeric PrP/total PrP was obtained by dividing the intensity of fraction 7 by the intensity of pre-column samples. In PPS(–) cases, the indices of oligomeric PrP/total PrP were increased according to the disease severity (Fig. 6A). Among PPS(+) cases, two CJD cases (cases 1 and 2) showed lower indices of oligomeric PrP/total PrP in comparison to PPS(–) cases. The indices of monomeric PrP/total PrP were decreased markedly in the cases with severe brain weight loss (Fig. 6B). There were no significant differences in the monomer indices between PPS(+) cases and PPS(–) cases.

DISCUSSION

Our post mortem study revealed that the PPS treatment did not apparently improve brain pathology in human prion diseases, although PPS treatment decreased the ratios of PrP^{res}/total PrP and the indices of oligomeric PrP/total PrP in some CJD cases. These findings might be relevant to apparently discrepant clinical findings: one reported no significant clinical improvements in prion diseases with PPS treatment[14,23] and the other reported that longer mean survival time in patients that had received PPS treatment was longer than previously reported for untreated specific prion diseases.[15]

The post mortem examinations revealed that neuronal loss, spongiform change and gliosis were advanced in both PPS(–) and PPS(+) cases with a greater loss of brain weight. In all PPS(+) cases, astrocytosis was evident in all layers of cerebral cortices, but GFAP expression levels were markedly reduced in the cerebral cortices, except in subpial astrocytes. CJD cases without PPS treatment usually showed strong immunoreactivity for GFAP in the cortical astrocytes as observed in case 5. Thus, we treated rat primary astrocytes with several concentrations of PPS (0 μg/mL, 0.4 μg/mL, 2.0 μg/mL, 10 μg/mL), but GFAP

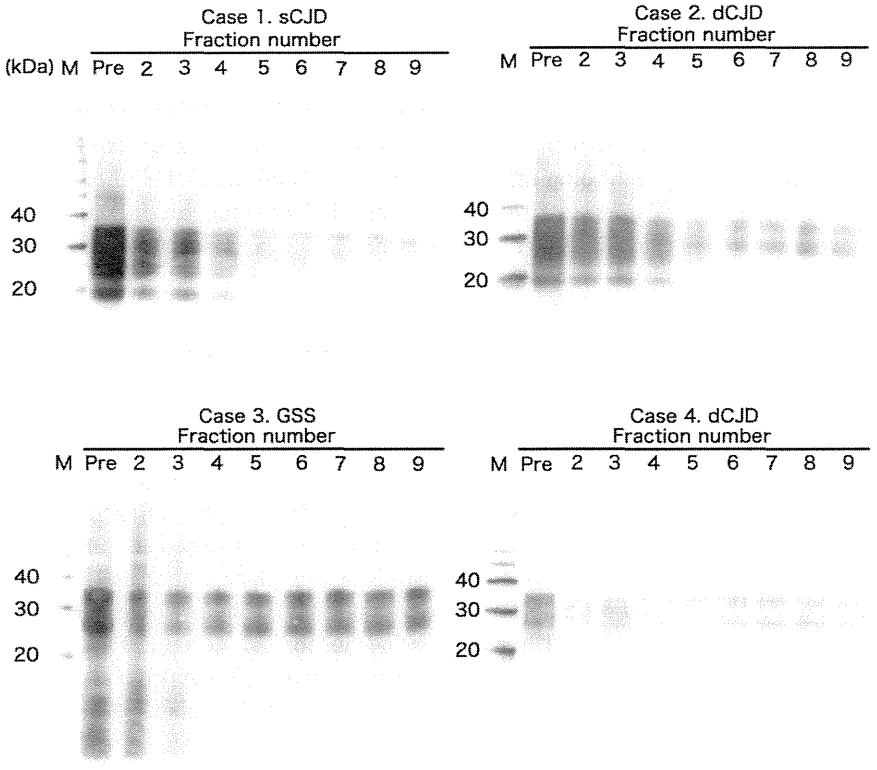

Fig. 5 Fractionation patterns of PrP in prion disease cases treated with PPS. The brain homogenate from the frontal cortex of each case was gel-filtrated without proteinase K (PK) treatment. Oligomeric PrP are detected mainly in fractions 2–4. Monomeric PrP are detected mainly in fractions 6–8. Pre: Pre-column brain homogenate.

expression levels were not significantly altered (data not shown). Therefore, we suggest that decreased GFAP expression levels in cortical astrocytes in PPS(+) cases is not due to the direct action of PPS on astrocytes.

PPS(+) cases in our study included only one case of sCJD (case 1). Although PPS infusion was started 3 months after disease onset, case 1 did not show any improvement in clinical features and the ratio of PrP^{res}/total PrP was comparable with PPS(−) sCJD cases. Meanwhile, two PPS(+) cases (cases 2 and 3) showed a relatively low ratio of PrP^{res}/total PrP. Because case 2 (dCJD) showed synaptic-type PrP deposition and type 1 PrP^{res} accumulation, it was considered to be a referential case to compare with PPS(−) CJD cases. Terada *et al.* also reported a reduction of PrP^{res} in a sCJD brain with PPS treatment.[23] In case 3 with GSS, PrP^{res} signals were very faint. It is possible that the molecular weights of plaque-type PrP deposition were too large to be detected through electrophoresis in these gels. Parchi *et al.* reported that immunoblot analysis of GSS P102L patients showed two major PrP^{res} signals with molecular masses of 21 and 8 kDa, and that the GSS patients with only the 8 kDa fragment showed mainly plaque-type PrP deposition.[24] In our study, the GSS patient with a P102L mutation showed both plaque-type PrP deposition and synaptic deposition, although Western blotting with PK treatment showed only PrP^{res} around 8 kDa. In this case, PrP^{res} might have a low resistance to PK treatment. Therefore, it may not be appropriate to compare the ratio of PrP^{res}/total PrP of case 3 to those of PPS(−) CJD cases. In case 4 with dCJD with plaque-type PrP deposits, Western blot analysis detected PrP^{res} fragments with intermediate size between types 1 and 2. Kobayashi *et al.* reported that the intermediate type PrP^{res} was seen in all examined dCJD cases with 129 methionine/methionine and plaque-type PrP deposits.[25]

Among PPS(+) cases, cases 1 and 2 showed lower indices of oligomeric PrP/total PrP than the indices of PPS(−) cases. PPS treatment might have reduced oligomeric PrP by reducing PrP^{res}. Alternatively, another study has reported that PrP fragments form amyloid aggregates in the presence of heparin which has a similar effect to PPS.[26] Therefore, oligomeric PrP in PPS(+) may be accumulated into fibrils. In our study, we did not evaluate fibrils because fibrils are difficult to electrophorese. Contrary to the reduction of oligomeric PrP/total PrP indices, monomeric PrP/total PrP indices in PPS(+) cases showed similar values to PPS(−) cases. The indices of monomeric PrP/total PrP were decreased, especially in cases with a brain weight of less than 1000 g. In these cases, PrP^{c} may have been depleted because of severe neuronal loss. Recently, oligomeric PrP was reported as the most infectious unit[17] and another study suggested that oligomeric PrP specifically inhibits the 26S proteasome, thus mediating a mechanism for intracellular neurotoxicity.[18]

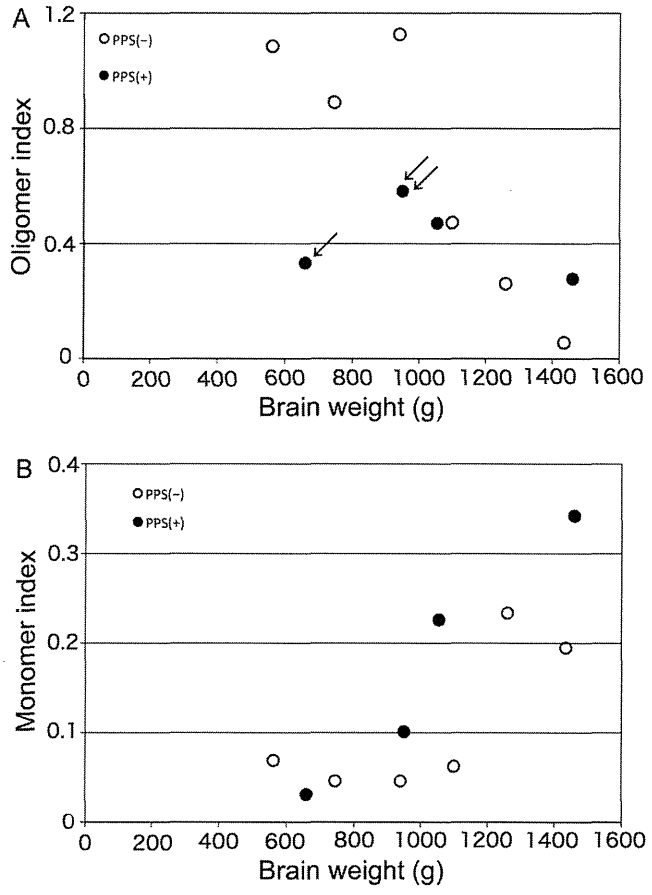

Fig. 6 Relationship between oligomeric PrP/total PrP indices and brain weight (A), or between monomeric PrP/total PrP indices and brain weight (B). (A) The oligomeric PrP/total PrP index was calculated by comparing the signals of fraction 3 to the signals of pre-column samples. In pentosan polysulfate negative (PPS(−)) cases (open circles), the oligomeric/total PrP indices are increased in accordance with brain weight loss. This tendency is also found in the PPS(+) cases (closed circles). The oligomeric PrP/total PrP indices in the PPS(+) cases are relatively low, particularly in the advanced cases with severe brain atrophy (case 1 (arrow) and case 2 (double arrows)). (B) The monomeric PrP/total PrP indices were calculated by comparing the signals of fraction 7 to the signals of pre-column samples. Monomeric PrP/total PrP indices of the advanced cases with severe brain atrophy are decreased irrespective of PPS treatment.

Doh-ura *et al.* reported that PPS infusion not only decreased PrP deposition but also reduced neurodegenerative changes in a rodent model.[9] However, in the rodent model PPS treatment could be started at the preclinical stage, whereas PPS treatment for patients was usually started at an advanced clinical stage. In the animal model, PPS treatment at an early or a late preclinical stage of the infection prolonged the incubation time by 2.4 or 1.7 times that of the control mice. Furthermore, the dosage of PPS in the animal model (460 μg/kg/day) was higher than the dosage for the human cases (120 μg/kg/day at a maximum).[9] Thus, if we could start PPS treatment at an earlier clinical stage or administer prophylactic PPS, the treatment might have beneficial effects on patients with prion diseases as shown in the experimental animal model.[9] Indeed the low indices of oligomeric PrP/total PrP were detected in two cases, but these cases showed no apparent clinicopathological improvements. Therefore, the therapeutic effects of intraventricular PPS infusion for human prion diseases are still uncertain.

ACKNOWLEDGMENTS

This work was funded by Grants-in-Aid for Scientific Research (B) (No. 22300116) and (C) (No. 21500337) from the Japan Society for the Promotion of Science (JSPS) and by the Health and Labor Sciences Research Grants (Research on Measures for Intractable Diseases) from the Ministry of Health, Labor and Welfare of Japan. The authors thank Ms Sachiko Koyama for her technical assistance. The authors also thank Drs Yoshio Tsuboi, Nobutaka Ishizu, Hiroshi Kurisaki and Shigeo Murayama for providing clinical data and pathological materials.

REFERENCES

1. Creutzfeldt HG. On a particular focal disease of the central nervous system (preliminary communication), 1920. *Alzheimer Dis Assoc Disord* 1989; **3**: 3–25.
2. Prusiner SB. Prions. *Proc Natl Acad Sci USA* 1998; **95**: 13363–13383.
3. Doh-Ura K, Iwaki T, Caughey B. Lysosomotropic agents and cysteine protease inhibitors inhibit scrapie-associated prion protein accumulation. *J Virol* 2000; **74**: 4894–4897.
4. Korth C, May BC, Cohen FE, Prusiner SB. Acridine and phenothiazine derivatives as pharmacotherapeutics for prion disease. *Proc Natl Acad Sci USA* 2001; **98**: 9836–9841.
5. Barret A, Tagliavini F, Forloni G *et al.* Evaluation of quinacrine treatment for prion diseases. *J Virol* 2003; **77**: 8462–8469.
6. Collins SJ, Lewis V, Brazier M, Hill AF, Fletcher A, Masters CL. Quinacrine does not prolong survival in a murine Creutzfeldt-Jakob disease model. *Ann Neurol* 2002; **52**: 503–506.
7. Collinge J, Gorham M, Hudson F *et al.* Safety and efficacy of quinacrine in human prion disease (PRION-1 study): a patient-preference trial. *Lancet Neurol* 2009; **8**: 334–344.
8. Caughey B, Brown K, Raymond GJ, Katzenstein GE, Thresher W. Binding of the protease-sensitive form of

PrP (prion protein) to sulfated glycosaminoglycan and congo red [corrected]. *J Virol* 1994; **68**: 2135–2141.
9. Doh-ura K, Ishikawa K, Murakami-Kubo I *et al.* Treatment of transmissible spongiform encephalopathy by intraventricular drug infusion in animal models. *J Virol* 2004; **78**: 4999–5006.
10. Caughey B, Raymond GJ. Sulfated polyanion inhibition of scrapie-associated PrP accumulation in cultured cells. *J Virol* 1993; **67**: 643–650.
11. Shyng SL, Lehmann S, Moulder KL, Harris DA. Sulfated glycans stimulate endocytosis of the cellular isoform of the prion protein, PrPC, in cultured cells. *J Biol Chem* 1995; **270**: 30221–30229.
12. Todd NV, Morrow J, Doh-ura K *et al.* Cerebroventricular infusion of pentosan polysulphate in human variant Creutzfeldt-Jakob disease. *J Infect* 2005; **50**: 394–396.
13. Rainov NG, Tsuboi Y, Krolak-Salmon P, Vighetto A, Doh-Ura K. Experimental treatments for human transmissible spongiform encephalopathies: is there a role for pentosan polysulfate? *Expert Opin Biol Ther* 2007; **7**: 713–726.
14. Tsuboi Y, Doh-Ura K, Yamada T. Continuous intraventricular infusion of pentosan polysulfate: clinical trial against prion diseases. *Neuropathology* 2009; **29**: 632–636.
15. Bone I, Belton L, Walker AS, Darbyshire J. Intraventricular pentosan polysulphate in human prion diseases: an observational study in the UK. *Eur J Neurol* 2008; **15**: 458–464.
16. Caughey B, Lansbury PT. Protofibrils, pores, fibrils, and neurodegeneration: separating the responsible protein aggregates from the innocent bystanders. *Annu Rev Neurosci* 2003; **26**: 267–298.
17. Silveira JR, Raymond GJ, Hughson AG *et al.* The most infectious prion protein particles. *Nature* 2005; **437**: 257–261.
18. Kristiansen M, Deriziotis P, Dimcheff DE *et al.* Disease-associated prion protein oligomers inhibit the 26S proteasome. *Mol Cell* 2007; **26**: 175–188.
19. Minaki H, Sasaki K, Honda H, Iwaki T. Prion protein oligomers in Creutzfeldt-Jakob disease detected by gel-filtration centrifuge columns. *Neuropathology* 2009; **29**: 536–542.
20. Lue LF, Kuo YM, Roher AE *et al.* Soluble amyloid beta peptide concentration as a predictor of synaptic change in Alzheimer's disease. *Am J Pathol* 1999; **155**: 853–862.
21. Sharon R, Bar-Joseph I, Frosch MP, Walsh DM, Hamilton JA, Selkoe DJ. The formation of highly soluble oligomers of alpha-synuclein is regulated by fatty acids and enhanced in Parkinson's disease. *Neuron* 2003; **37**: 583–595.
22. Sasaki K, Minaki H, Iwaki T. Development of oligomeric prion-protein aggregates in a mouse model of prion disease. *J Pathol* 2009; **219**: 123–130.
23. Terada T, Tsuboi Y, Obi T *et al.* Less protease-resistant PrP in a patient with sporadic CJD treated with intraventricular pentosan polysulphate. *Acta Neurol Scand* 2010; **121**: 127–130.
24. Parchi P, Chen SG, Brown P *et al.* Different patterns of truncated prion protein fragments correlate with distinct phenotypes in P102L Gerstmann-Straussler-Scheinker disease. *Proc Natl Acad Sci USA* 1998; **95**: 8322–8327.
25. Kobayashi A, Asano M, Mohri S, Kitamoto T. Cross-sequence transmission of sporadic Creutzfeldt-Jakob disease creates a new prion strain. *J Biol Chem* 2007; **282**: 30022–30028.
26. Cortijo-Arellano M, Ponce J, Durany N, Cladera J. Amyloidogenic properties of the prion protein fragment PrP(185-208): comparison with Alzheimer's peptide Abeta(1-28), influence of heparin and cell toxicity. *Biochem Biophys Res Commun* 2008; **368**: 238–242.

Eur J Nucl Med Mol Imaging (2013) 40:125–132
DOI 10.1007/s00259-012-2261-2

ORIGINAL ARTICLE

Comparison of the binding characteristics of [^{18}F]THK-523 and other amyloid imaging tracers to Alzheimer's disease pathology

Ryuichi Harada · Nobuyuki Okamura · Shozo Furumoto · Tetsuro Tago · Masahiro Maruyama · Makoto Higuchi · Takeo Yoshikawa · Hiroyuki Arai · Ren Iwata · Yukitsuka Kudo · Kazuhiko Yanai

Received: 1 May 2012 / Accepted: 21 September 2012 / Published online: 26 October 2012

Abstract
Purpose Extensive deposition of senile plaques and neurofibrillary tangles in the brain is a pathological hallmark of Alzheimer's disease (AD). Although several PET imaging agents have been developed for in vivo detection of senile plaques, no PET probe is currently available for selective detection of neurofibrillary tangles in the living human brain. Recently, [^{18}F]THK-523 was developed as a potential in vivo imaging probe for tau pathology. The purpose of this study was to compare the binding properties of [^{18}F]THK-523 and other amyloid imaging agents, including PiB, BF-227 and FDDNP, to synthetic protein fibrils and human brain tissue.
Methods In vitro radioligand binding assays were conducted using synthetic amyloid β_{42} and K18ΔK280-tau fibrils. Nonspecific binding was determined by the addition of unlabelled compounds at a concentration of 2 μM. To examine radioligand binding to neuropathological lesions, in vitro autoradiography was conducted using sections of AD brain.
Results [^{18}F]THK-523 showed higher affinity for tau fibrils than for Aβ fibrils, whereas the other probes showed a higher affinity for Aβ fibrils. The autoradiographic analysis indicated that [^{18}F]THK-523 accumulated in the regions containing a high density of tau protein deposits. Conversely, PiB and BF-227 accumulated in the regions containing a high density of Aβ plaques.
Conclusion These findings suggest that the unique binding profile of [^{18}F]THK-523 can be used to identify tau deposits in AD brain.

Keywords PET probes · Tau · Amyloid · Alzheimer's disease

Electronic supplementary material The online version of this article (doi:10.1007/s00259-012-2261-2) contains supplementary material, which is available to authorized users.

R. Harada · N. Okamura (✉) · S. Furumoto · T. Yoshikawa · K. Yanai
Department of Pharmacology,
Tohoku University School of Medicine,
2-1, Seiryo-machi, Aoba-ku,
Sendai 980-8575, Japan
e-mail: nookamura@med.tohoku.ac.jp

S. Furumoto · T. Tago · R. Iwata
Division of Radiopharmaceutical Chemistry,
Cyclotron and Radioisotope Center, Tohoku University,
Sendai, Japan

M. Maruyama · M. Higuchi
Molecular Imaging Center, National Institute
of Radiological Sciences,
Chiba, Japan

H. Arai
Department of Geriatrics and Gerontology, Institute of
Development, Aging and Cancer, Tohoku University,
Sendai, Japan

Y. Kudo
Innovation of New Biomedical Engineering Center,
Tohoku University,
Sendai, Japan

Introduction

Senile plaques and neurofibrillary tangles (NFTs) composed of amyloid-β (Aβ) peptides and aggregated tau proteins, respectively, are the pathological hallmarks of

Alzheimer's disease (AD). In vivo amyloid imaging techniques have received a lot of attention for their promise in presymptomatic detection of Aβ pathology [1]. Recently, several β-sheet binding radiotracers have been developed as PET amyloid imaging agents [2]. Among them, ^{18}F-labelled 2-(1-{6-[(2-fluoroethyl(methyl)amino)-2-naphthyl)ethylidene)malononitrile ([^{18}F]FDDNP) was the first PET probe to be applied to clinical PET imaging in patients with AD [3]. This tracer demonstrated higher regional uptake in the medial temporal lobe and neocortex, and was claimed to bind to Aβ and tau pathological lesions [3]. Subsequently, ^{11}C-labelled 2-[4′-(methylamino)phenyl]-6-hydroxybenzothiazole ([^{11}C]PiB) and 2-(2-[dimethylaminothiazole-5-yl]ethenyl)-6-(2-[fluoro]ethoxy)benzoxazole ([^{11}C]BF-227) were also developed as amyloid imaging radiotracers. These tracers bind to Aβ fibrils with high affinity [4] and have demonstrated a significantly higher retention in the neocortical areas of brains of AD patients than of healthy controls [5, 6]. Furthermore, post-mortem analysis of AD patients who had undergone [^{11}C]PiB PET imaging before death suggested a strong correlation between in vivo PiB binding and regional distribution of Aβ plaques [7].

Amyloid imaging with PET can detect AD pathology in its preclinical stage [8]. However, amyloid deposition as assessed by [^{11}C]PiB PET correlates poorly with cognitive impairment in AD [9, 10], whereas deposition of tau in the medial temporal cortex is closely associated with neuronal death in this region. Selective tau imaging would provide important information about the tau pathophysiological features in AD, allowing correlation of brain tau load with cognitive decline, monitoring of disease progression and evaluation of therapeutic efficacy of newly developed therapies. Potential candidates for in vivo tau imaging agents include quinoline derivatives [11], and in a recent study, we found that one quinoline derivative, [^{18}F]THK-523, showed higher affinity for tau rather than amyloid fibrils. Furthermore, an autoradiography analysis indicated that this tracer binds specifically to tau deposits but not Aβ burden at tracer concentrations usually achieved during a PET scan [12].

The binding profiles of PiB, BF-227 and FDDNP to Aβ fibrils have been well described. Because tau, α-synuclein and prion fibrils, as well as Aβ fibrils, share a common β-sheet secondary structure, these compounds can potentially bind all these misfolded proteins. A previous study indicated that PiB binds to both Aβ and PHF tau pathology in vitro [13]. However, the binding occurs at higher concentrations than usually achieved in vivo during a PET scan. Furthermore, PET–pathology correlation studies have demonstrated that PiB binding reflects Aβ pathology [7, 14]. Newly developed ^{18}F-labelled amyloid PET tracers have similarly shown good correlation with Aβ plaque density [15, 16]. However, the binding affinity of these radiotracers for tau fibrils remains unknown and the binding properties of [^{18}F]THK-523 have not been directly compared with those of other amyloid PET agents. Here, we compared the binding affinity of [^{18}F]THK-523 to synthetic Aβ and tau protein fibrils as well as to senile plaques and NFTs in human brain samples with those of PiB, BF-227 and FDDNP, to characterize the binding properties of THK-523 and to obtain a better understanding of current and future PET data.

Materials and methods

Materials

The nonlabelled compounds PiB, BF-227, FDDNP, THK-523 (Fig. 1) and their precursors were custom-synthesized by Tanabe R&D Service (Osaka, Japan). Human $Aβ_{42}$ was purchased from Peptide Institute Inc. (Mino, Japan). Recombinant K18ΔK280-tau protein was obtained from Invitrogen (Tokyo, Japan).

Radiolabelling of PiB, BF-227, THK-523 and FDDNP

[^{3}H]PiB (specific activity 2.96 GBq/μmol) was purchased from American Radiolabeled Chemicals (St. Louis, MO). [^{11}C]PiB was radiolabelled using its precursor (2-(4-aminophenyl)-6-methoxymethoxybenzothiazole) and [^{11}C]methyl triflate, as

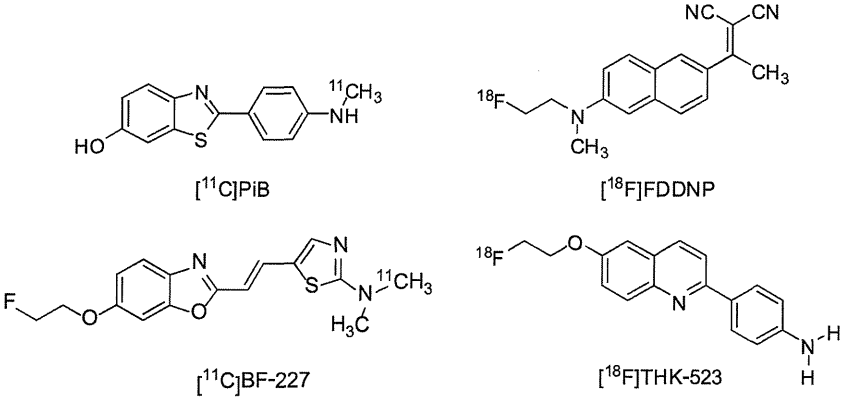

Fig. 1 Chemical structures of [^{11}C]PiB, [^{18}F]FDDNP, [^{11}C]BF-227 and [^{18}F]THK-523

previously described [17, 18]. The mean specific activity of [^{11}C]PiB was 34.6 GBq/μmol.

[^{18}F]BF-227 was synthesized by nucleophilic substitution of the tosylate precursor (2-[2-(2-dimethylaminothiazol-5-yl)ethenyl]-6-[2-(tosyloxy)ethoxy]benzoxazole. After a 10-min reaction at 110 °C, the crude mixture was partially purified on an activated Sep-Pak tC18 cartridge before being purified by semipreparative reverse-phase HPLC. Standard tC18 Sep-Pak reformulation produced [^{18}F]BF-227 in >95 % purity. The radiochemical yield was 12–19 % (non-decay-corrected), and the mean specific activity of [^{18}F]BF-227 was 163 GBq/μmol at the end of the synthesis. [^{11}C]BF-227 was synthesized using *N*-desmethylated derivatives as its precursor and [^{11}C]methyl triflate, as previously described [6]. The mean specific activity of [^{11}C]BF-227 was 136 GBq/μmol.

[^{18}F]THK-523 was synthesized by nucleophilic substitution of the tosylate precursor (2-(4-aminophenyl)-6-(2-tosyloxyethoxy)quinolone) as previously described [12]. The standard tC18 Sep-Pak reformulation produced [^{18}F]THK-523 in >95 % purity. The radiochemical yield was 38–49 % (non-decay-corrected), and the mean specific activity of [^{18}F]THK-523 was 68 GBq/μmol at the end of the synthesis.

[^{18}F]FDDNP was radiolabelled by the nucleophilic substitution of the tosylate precursor (2-{[6-(2,2-dicyano-1-methylvinyl)-2-naphthyl](methyl)amino}ethyl-4-methylbenzenesulphonate) as previously described [19]. After a 15-min reaction at 95 °C, the crude mixture was partially purified on an activated Sep-Pak tC18 cartridge before being purified by semipreparative reverse-phase HPLC. Standard tC18 Sep-Pak reformulation produced [^{18}F]FDDNP in >95 % purity. The radiochemical yield was 12–19 % (non-decay-corrected), and the mean specific activity of [^{18}F]FDDNP was 27 GBq/μmol at the end of the synthesis. All analysis HPLC chromatograms are shown in the Supplementary figure.

In vitro radioligand binding assays

Synthetic $A\beta_{42}$ fibrils and K18ΔK280-tau fibrils were prepared as previously described [12]. For in vitro binding assays, synthetic $A\beta_{42}$ or K18ΔK280 fibrils (200 nM) were incubated with increasing concentrations of [^{3}H]PiB and ^{18}F-labelled compounds (0.5–200 nM). To account for nonspecific binding of [^{3}H]PiB and ^{18}F-labelled compounds, the above-mentioned reactions were performed in triplicate in the presence of each unlabelled compound at a concentration of 2 μM.

The binding reactions were incubated for 1 h for the ^{18}F-labelled compounds and 3 h for [^{3}H]PiB at room temperature, in 200 μL of assay buffer (Dulbecco's PBS, 0.1 % BSA). Separation of bound from free radioactivity was achieved by filtration under reduced pressure (MultiScreen HTS Vacuum Manifold, MultiScreen HTS 96-well 0.65-μm filtration plate; Millipore, Billerica, MA). The filters were washed three times with 200-μL assay buffer, and the filters containing the bound ^{18}F-labelled compounds were then assayed for radioactivity in a γ counter (AccuFLEX γ7000, Aloka, Tokyo, Japan). The filters containing [^{3}H]PiB were incubated in 2 mL of scintillation fluid (Aquasol-2; PerkinElmer, Boston, MA), and the radioactivity of ^{3}H was counted using a β counter (LS6500 liquid scintillation counter; Beckman Coulter, Brea, CA). The binding data were analysed with curve-fitting software that calculated the K_D and B_{max} using nonlinear regression (GraphPad Prism version 5.0; GraphPad Software, San Diego, CA).

Autoradiography, immunohistochemistry and Gallyas silver staining

Demographics of post-mortem brain samples are shown in Table 1. The frontal and medial temporal brain sections (6 μm thick) of three AD patients were incubated with 1.0 MBq/mL ^{11}C-labelled and ^{18}F-labelled compounds at room temperature for 10 min and then washed briefly with water and 50 % ethanol. After drying, the labelled sections were exposed to a BAS-III imaging plate (Fuji Film, Tokyo, Japan) overnight. The autoradiographic images were obtained using a BAS-5000 phosphoimaging instrument (Fuji Film) with a spatial resolution of 25×25 μm. The adjacent sections were immunostained using AT8 anti-tau monoclonal antibody (diluted 1:20; Innogenetics, Ghent, Belgium) and 6F/3D (diluted 1:50; Dako, Glostrup, Denmark). The adjacent sections were also stained by the Gallyas-Braak method, which has been reported to be NFT-specific [20].

Results

Binding affinity for synthetic Aβ and tau fibrils

To characterize the binding properties of THK-523, PiB, BF-227 and FDDNP, in vitro radioligand binding assays for synthetic $A\beta_{42}$ and truncated tau construct (K18ΔK280) fibrils were performed under the same experimental conditions. Truncated tau construct (K18ΔK280) consists of the four repeat regions (244–372) but lacking lysine 280 (ΔK280) observed in FTLD-17 familial mutation.

Table 1 Demographics of brain samples used in this study

Brain no.	Age (years)	Sex	Post-mortem interval (h)
AD1	76	F	16
AD2	82	F	17
AD3	92	F	8.5

K18ΔK280 tau aggregates exhibit the similar characteristic as PHF-tau from AD brain [21]. In addition, K18ΔK280 tau forms aggregates quickly without cofactor such as heparin [22]. Thus, we used K18ΔK280 fibrils for the in vitro binding assays. Our analysis indicated that [^{18}F]THK-523 had a higher binding affinity for tau fibrils (K_{D1} = 1.99 ± 0.21 nM, B_{max1} = 1.22 ± 0.24 pmol THK-523/nmol K18ΔK280-tau) than for $A\beta_{42}$ fibrils (K_{D1} = 30.3 ± 3.91 nM, B_{max1} = 12.6 ± 0.45 pmol THK-523/nmol $A\beta_{42}$), which was similar to previously published data [12]. On the other hand, [^{3}H]PiB bound to $A\beta_{42}$ fibrils with high affinity (K_{D1} = 0.84 ± 0.18 nM, B_{max1} = 0.44 ± 0.07 pmol PiB/nmol $A\beta_{42}$). [^{3}H]PiB also showed two binding sites for K18ΔK280-tau fibrils, but with a lower affinity (K_{D1} = 6.39 ± 1.63 nM, B_{max1} = 1.38 ± 0.48 pmol PiB/nmol K18ΔK280) than [^{18}F]THK-523. [^{18}F]BF-227 showed a high binding affinity for $A\beta_{42}$ fibrils (K_{D1} = 1.72 ± 0.83 nM, B_{max1} = 0.50 ± 0.14 pmol BF-227/nmol $A\beta_{42}$), similar to our previous report [23], but showed a lower affinity for tau fibrils (K_D = 30.2 ± 2.29 nM, B_{max} = 10.7 ± 0.24 pmol BF-227/nmol K18ΔK280-tau). [^{18}F]BF-227 had an approximately 20-fold higher affinity for the first class of $A\beta_{42}$ binding sites compared with tau fibrils. Only one class of [^{18}F]FDDNP binding site was identified on the $A\beta_{42}$ (K_D = 5.52 ± 1.97 nM, B_{max} = 0.277 ± 0.06 pmol FDDNP/nmol $A\beta_{42}$) and K18ΔK280 tau fibrils (K_D = 36.7 ± 11.6 nM, B_{max} = 2.14 ± 0.46 pmol FDDNP/nmol K18ΔK280-tau). These results suggest that [^{18}F]FDDNP binds $A\beta_{42}$ fibrils with lower affinity than [^{3}H]PiB and [^{18}F]BF-227. Furthermore, [^{18}F]FDDNP had an approximately sevenfold higher affinity for $A\beta_{42}$ fibrils than for tau fibrils. These binding profiles are significantly different from that of [^{18}F]THK-523 (Table 2).

In vitro autoradiography of human brain sections

To further assess the binding selectivity of [^{18}F]THK-523, autoradiographic images of the frontal (Fig. 2) and medial temporal (Fig. 3) brain sections from three AD patients, using [^{18}F]THK-523, [^{11}C]PiB and [^{11}C]BF-227, were compared. While Aβ plaques in the frontal grey matter were labelled with [^{11}C]PiB (Fig. 2a–c) and [^{11}C]BF-227 (Fig. 2g–i), the binding of [^{18}F]THK-523 in the frontal grey matter (Fig. 2m–o) was considerably lower. In the medial temporal brain sections, [^{11}C]PiB (Fig. 3a–c) and [^{11}C]BF-227 (Fig. 3g–i) did not accumulate in the hippocampal CA1 area, whereas [^{18}F]THK-523 (Fig. 3m–o) did accumulate in this area (Fig. 3m–o). The presence of a high density of tau and a low density of Aβ in this area was confirmed by immunohistochemistry (Fig. 3d–f, j–l). Furthermore, the band-like distribution of [^{18}F]THK-523 in the inner layer of the temporal grey matter was similar to the distribution of tau (Fig. 3j–l). In the high-magnification images of case AD3 (Fig. 3p–v), the distribution of [^{18}F]THK-523 closely resembled Gallyas silver staining and tau immunostaining. [^{18}F]THK-523 binding was observed in the areas showing a high density of NFTs in the hippocampal CA1, the layer pre-α and pri-α in the entorhinal cortex (ERC) (Fig. 3p, q, r, t). Intriguingly, [^{18}F]THK-523 labelling in the layer pre-α of the ERC corresponded to Gallyas silver staining better than tau immunostaining, suggesting the preferential binding of [^{18}F]THK-523 to extracellular tau deposits that were clearly visualized by Gallyas silver staining [25]. In contrast to [^{18}F]THK-523, the distribution of [^{11}C]PiB was similar to that of Aβ immunohistochemistry (Fig 3q, u, v). [^{11}C]PiB binding corresponded to the formation of amyloid in the parvopyramidal layer of the presubicular area and in the layers pre-β and pre-γ of the ERC (Fig. 3s, v) [26].

Discussion

In the study reported here, we for the first time directly compared the binding properties of the novel quinoline derivative THK-523 and other amyloid PET probes. Our data suggest the potential utility of THK-523 for the selective detection of PHF-tau in the living human brain, which has not previously been achieved. The autoradiographic images of sections from AD brains revealed that [^{18}F]THK-523 successfully labelled PHF-tau deposits but did not label Aβ deposits in the frontal and temporal cortices. These findings suggest that [^{18}F]THK-523 is a promising

Table 2 K_D and B_{max} values of [^{3}H]PiB, [^{18}F]BF-227, [^{18}F]FDDNP and [^{18}F]THK-523 for K18ΔK280-tau and $A\beta_{42}$ fibrils

Compound	K18ΔK280 fibrils				$A\beta_{42}$ fibrils			
	K_{D1}	B_{max1}	K_{D2}	B_{max2}	K_{D1}	B_{max1}	K_{D2}	B_{max2}
[^{18}F]THK-523	1.99±0.21	1.22±0.24	50.7±2.73	4.55±0.74	30.3±3.91	12.6±0.45	–	–
[^{18}F]BF-227	30.2±2.29	10.7±0.24	–	–	1.72±0.83	0.50±0.14	56.1±25.1	13.4±4.37
[^{18}F]FDDNP	36.7±11.6	2.14±0.46	–	–	5.52±1.97	0.277±0.06	–	–
[^{3}H]PiB	6.39±1.63	1.38±0.48	304±77.4	20.6±11.2	0.84±0.18	0.44±0.07	60.6±8.32	26.1±8.57

K_D values are in nanomoles, and B_{max} values are in picomoles compound per nanomole fibrils (n=3).

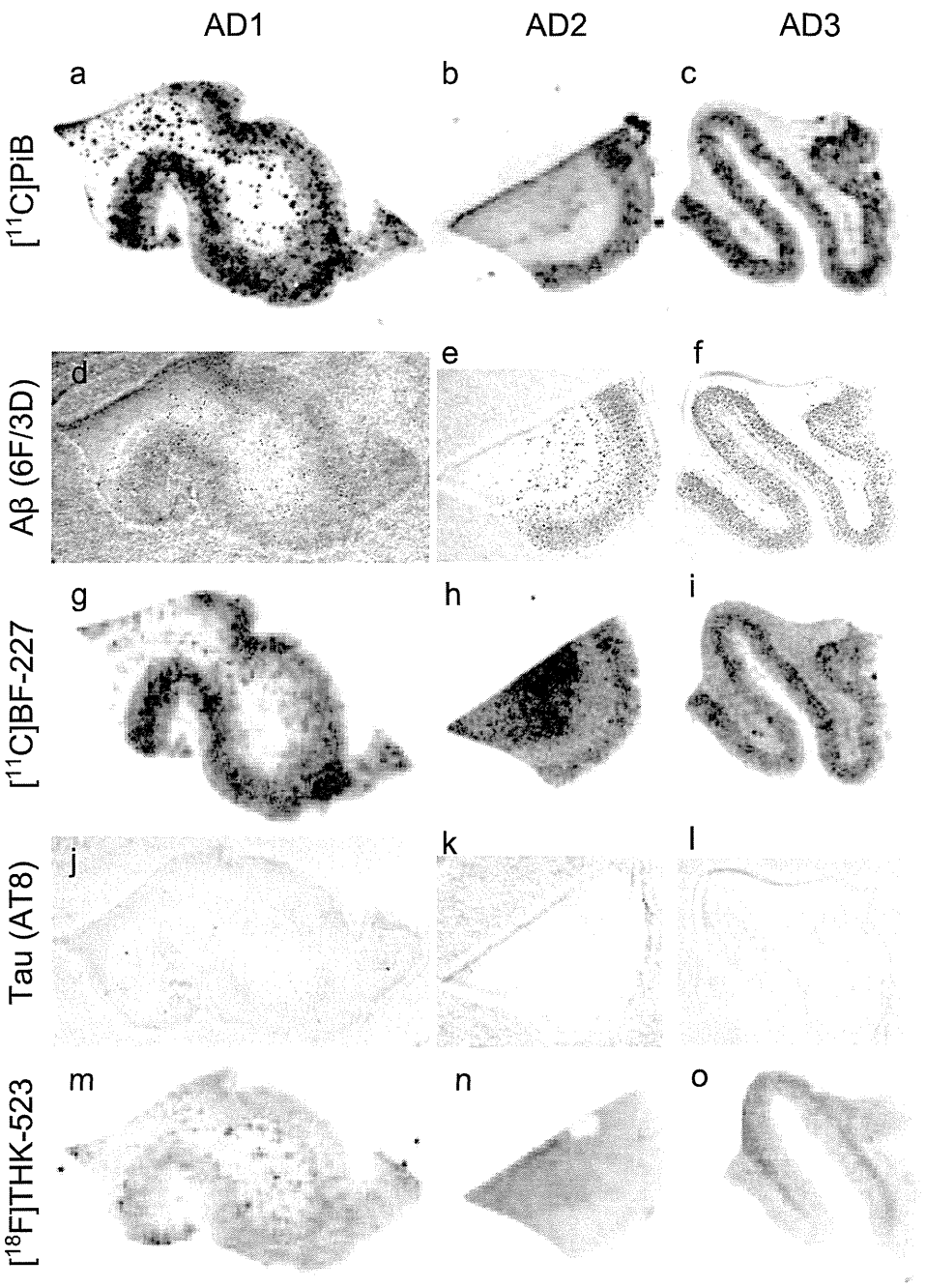

Fig. 2 Comparison of [^{11}C]PiB, [^{11}C]BF-227 and [^{18}F]THK-523 autoradiography with the Aβ and tau immunostaining in sections of the frontal brain from three patients with AD (*AD1*, *AD2*, *AD3*). Both [^{11}C]PiB (**a–c**) and [^{11}C]BF-227 (**g–i**) showed dense accumulation in the grey matter, closely resembling the pattern of Aβ immunohistochemistry using the 6F/3D antibody (**d–f**). [^{18}F]THK-523 (**m–o**) did not accumulate in the grey matter, which was correlated with no marked staining with anti-tau antibody AT8 (**j–l**)

candidate as a tau imaging tracer, and could also be a lead compound for future development of tau-selective radiotracers. We speculate that [^{18}F]THK-523 would show retention in tau-rich brain regions if administered to AD patients. However, the specific signal of [^{18}F]THK-523 might be lower than those of PiB and BF-227 owing to the lower amount of tau deposits in the neocortex of AD patients [27]. Further compound optimization may be required to achieve higher contrast imaging of PHF-tau deposits.

In in vitro saturation binding studies [^{18}F]THK-523 bound with higher affinity to tau fibrils (K_{D1} 1.99 nM) than to $A\beta_{42}$ fibrils (K_{D1} 30.3 nM), whereas PiB and BF-227 showed the opposite binding characteristics. [^{3}H]PiB bound with higher affinity to $A\beta_{42}$ fibrils (K_{D1} 0.84 nM) than to tau fibrils (K_{D1} 6.39 nM), similar to previous reports [7, 28, 29], and [^{18}F]BF-227 had more than a tenfold higher affinity for $A\beta_{42}$ fibrils (K_{D1} 1.72 nM) than for tau fibrils (K18ΔK280; K_{D1} 30.2 nM). Autoradiographic images of sections of AD brain revealed that [^{11}C]PiB and [^{11}C]BF-227 accumulated in the grey matter of the neocortex, which closely resembled the staining pattern of Aβ immunohistochemistry. A previous study suggested that [^{3}H]PiB labelled NFTs at tracer concentrations usually achieved during a PET scan [13]. However, another study showed no binding of the PiB derivative [^{3}H]BTA-1 to

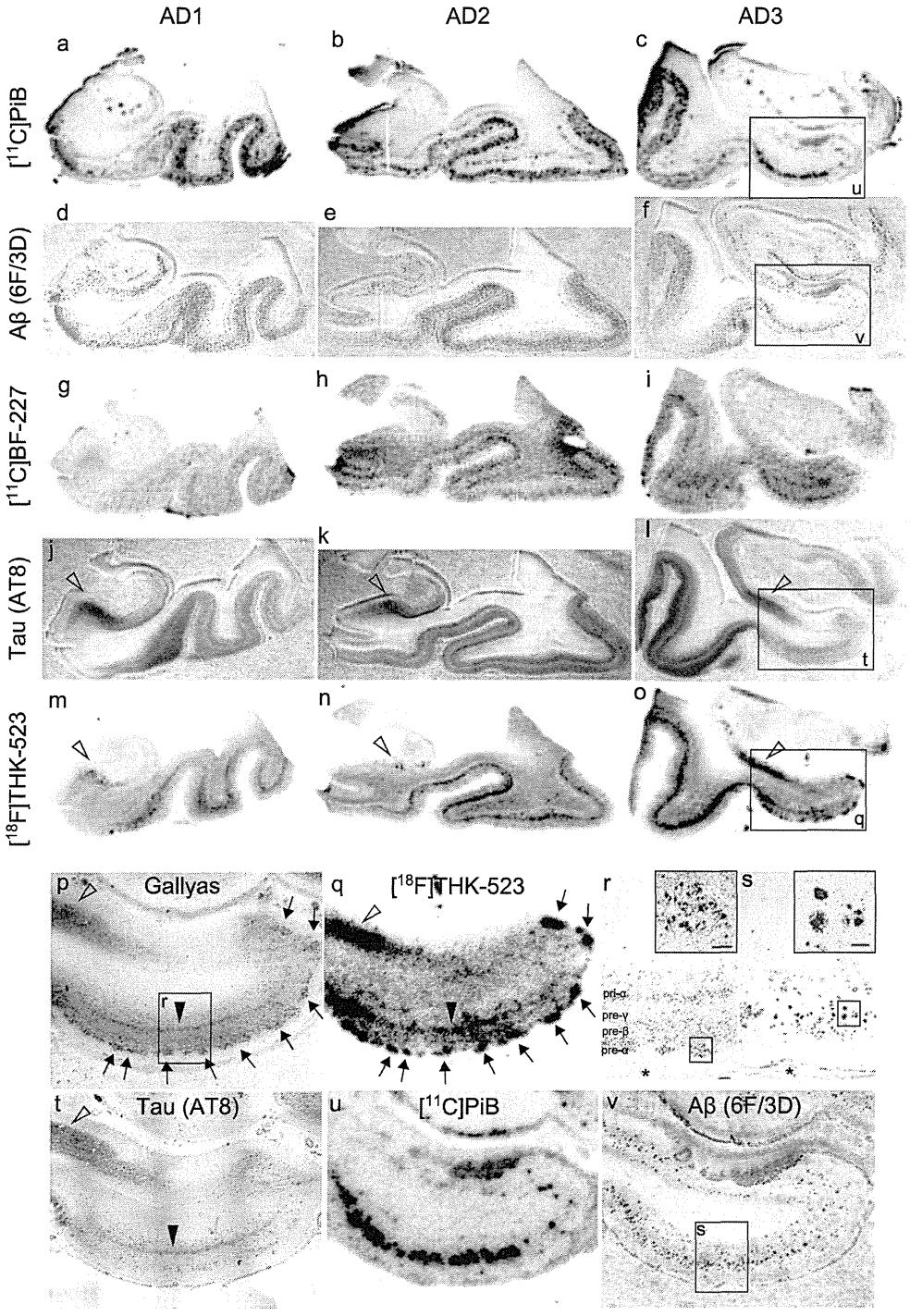

Fig. 3 Comparison of [^{11}C]PiB, [^{11}C]BF-227 and [^{18}F]THK-523 autoradiography with Aβ and tau immunostaining images in sections of the medial temporal brain from three patients with AD (*AD1*, *AD2*, *AD3*). [^{11}C]PiB (**a–c**) and [^{11}C]BF-227 (**g–i**) do not accumulate in the hippocampal CA1 area which contains a low density of Aβ (**d–f**). In contrast, accumulation of [^{18}F]THK-523 is observed in the hippocampal CA1 area (**m–o**, *arrowheads*), which closely resembles AT8 immunoreactivity (**j–l**, *arrowheads*). In addition, the band-like labelling pattern of [^{18}F]THK-523 in the inner layer of temporal cortex (**m–o**) is closely similar to that of AT8 immunostaining (**j–l**). **p–v** High magnification images of the medial temporal sections from patient AD3. Many clusters of [^{18}F]THK-523 binding in the ERC are consistent with Gallyas silver staining (**p**, **q**, *arrows*). **r** Close-up image from **p**. Numerous NFTs are located in the layer pre-α of the ERC (**r** *inset*). The band-like distribution of [^{18}F]THK-523 in the layer pri-α of the ERC also resembles the labelling pattern of Gallyas silver staining (**p**, *filled arrowhead*) as well as AT8 immunoreactivity (**t**, *filled arrowhead*). [^{11}C]PiB binding (**u**) is also present in the ERC, but obviously different from [^{18}F]THK-523 binding (**q**) and similar to the 6F/3D immunostaining pattern (**v**). Lake-like amyloid in the presubicular region (**v**) is labelled with [^{11}C]PiB, but not with [^{18}F]THK-523. **s** Close-up image from **v**. Aβ plaques (**s** *inset*) located in the layer pre-β and pre-γ are intensely labelled with [^{11}C]PiB (**u**). *Asterisks* in **r** and **s** denote the same large blood vessel. *Scale bar* 100 μm

plaque-free and NFT-rich ERC homogenates, despite the high amount of [^{3}H]BTA-1 binding to frontal cortex homogenates containing high levels of neuritic plaques [30]. Autoradiographic and immunohistochemical analyses indicated that PiB predominantly binds to senile plaques but not to NFTs. These findings are consistent with the findings from clinical PiB-PET studies showing no remarkable PiB retention in the medial temporal cortex of AD patients [7].

Another radiotracer, [^{18}F]FDDNP, has been reported to detect Aβ and tau pathological lesions in AD patients [3]. Previous clinical PET studies have shown higher cortical uptake of [^{18}F]FDDNP in the lateral and medial temporal lobes of AD subjects [3, 5]. Furthermore, a multitracer PET study of [^{11}C]PiB and [^{18}F]FDDNP has shown significant retention of FDDNP in the medial temporal cortex, albeit no remarkable retention of PiB in the same region [31]. However, in vitro binding studies have shown the limited binding affinity of [^{3}H]FDDNP to AD pathological lesions [24], and a previous autoradiographic analysis has suggested that [^{3}H]FDDNP does not significantly label any region in AD brain [24]. Previous in vitro binding studies additionally showed the binding affinity of FDDNP for $A\beta_{40}$ fibrils (K_D 0.12, 85 nM) [19, 24], but the binding affinity for tau fibrils was not reported. Here, we showed that the binding affinity of [^{18}F]FDDNP for tau fibrils (K_{D1} 36.7 nM) was similar to that of [^{18}F]BF-227 (K_{D1} 30.2 nM), but much higher than that of [^{18}F]THK-523 (K_{D1} 1.99 nM).

In conclusion, the binding profiles of [^{18}F]THK-523, [^{11}C]PiB, [^{18}F]BF-227, and [^{18}F]FDDNP were compared using in vitro saturation binding assays and autoradiography of sections of AD brain. These data suggest that [^{18}F]THK-523 shows a binding preference for tau protein fibrils. Therefore, [^{18}F]THK-523 is a candidate as a radiotracer to identify tau protein deposits and a lead compound for future tracer development. Ongoing clinical trials will clarify the clinical utility of this tracer and its derivatives for tau imaging in vivo.

Acknowledgments This study was supported by the Industrial Technology Research Grant Program of the NEDO in Japan, Health and Labor Sciences Research Grants from the Ministry of Health, Labor, and Welfare of Japan, and Grant-in-Aid for Scientific Research (B) (23390297).

References

1. Nordberg A, Rinne JO, Kadir A, Langstrom B. The use of PET in Alzheimer disease. Nat Rev Neurol. 2010;6:78–87. doi:10.1038/nrneurol.2009.217.
2. Furumoto S, Okamura N, Iwata R, Yanai K, Arai H, Kudo Y. Recent advances in the development of amyloid imaging agents. Curr Top Med Chem. 2007;7:1773–89.
3. Shoghi-Jadid K, Small GW, Agdeppa ED, Kepe V, Ercoli LM, Siddarth P, et al. Localization of neurofibrillary tangles and beta-amyloid plaques in the brains of living patients with Alzheimer disease. Am J Geriatr Psychiatry. 2002;10:24–35.
4. Mathis CA, Wang Y, Holt DP, Huang GF, Debnath ML, Klunk WE. Synthesis and evaluation of 11C-labeled 6-substituted 2-arylbenzothiazoles as amyloid imaging agents. J Med Chem. 2003;46:2740–54. doi:10.1021/jm030026b.
5. Klunk WE, Engler H, Nordberg A, Wang Y, Blomqvist G, Holt DP, et al. Imaging brain amyloid in Alzheimer's disease with Pittsburgh Compound-B. Ann Neurol. 2004;55:306–19. doi:10.1002/ana.20009.
6. Kudo Y, Okamura N, Furumoto S, Tashiro M, Furukawa K, Maruyama M, et al. 2-(2-[2-Dimethylaminothiazol-5-yl]ethenyl)-6- (2-[fluoro]ethoxy)benzoxazole: a novel PET agent for in vivo detection of dense amyloid plaques in Alzheimer's disease patients. J Nucl Med. 2007;48:553–61.
7. Ikonomovic MD, Klunk WE, Abrahamson EE, Mathis CA, Price JC, Tsopelas ND, et al. Post-mortem correlates of in vivo PiB-PET amyloid imaging in a typical case of Alzheimer's disease. Brain. 2008;131:1630–45. doi:10.1093/brain/awn016.
8. Sperling RA, Aisen PS, Beckett LA, Bennett DA, Craft S, Fagan AM, et al. Toward defining the preclinical stages of Alzheimer's disease: recommendations from the National Institute on Aging-Alzheimer's Association workgroups on diagnostic guidelines for Alzheimer's disease. Alzheimers Dement. 2011;7:280–92. doi:10.1016/j.jalz.2011.03.003.
9. Jack Jr CR, Knopman DS, Jagust WJ, Shaw LM, Aisen PS, Weiner MW, et al. Hypothetical model of dynamic biomarkers of the Alzheimer's pathological cascade. Lancet Neurol. 2010;9:119–28. doi:10.1016/S1474-4422(09)70299-6.
10. Pike KE, Savage G, Villemagne VL, Ng S, Moss SA, Maruff P, et al. Beta-amyloid imaging and memory in non-demented individuals: evidence for preclinical Alzheimer's disease. Brain. 2007;130:2837–44. doi:10.1093/brain/awm238.
11. Okamura N, Suemoto T, Furumoto S, Suzuki M, Shimadzu H, Akatsu H, et al. Quinoline and benzimidazole derivatives: candidate probes for in vivo imaging of tau pathology in Alzheimer's disease. J Neurosci. 2005;25:10857–62. doi:10.1523/JNEUROSCI.1738-05.2005.
12. Fodero-Tavoletti MT, Okamura N, Furumoto S, Mulligan RS, Connor AR, McLean CA, et al. 18F-THK523: a novel in vivo tau imaging ligand for Alzheimer's disease. Brain. 2011;134:1089–100. doi:10.1093/Brain/Awr038.
13. Lockhart A, Lamb JR, Osredkar T, Sue LI, Joyce JN, Ye L, et al. PIB is a non-specific imaging marker of amyloid-beta (Abeta) peptide-related cerebral amyloidosis. Brain. 2007;130:2607–15. doi:10.1093/brain/awm191.
14. Burack MA, Hartlein J, Flores HP, Taylor-Reinwald L, Perlmutter JS, Cairns NJ. In vivo amyloid imaging in autopsy-confirmed Parkinson disease with dementia. Neurology. 2010;74:77–84. doi:10.1212/WNL.0b013e3181c7da8e.
15. Clark CM, Schneider JA, Bedell BJ, Beach TG, Bilker WB, Mintun MA, et al. Use of florbetapir-PET for imaging beta-amyloid pathology. JAMA. 2011;305:275–83. doi:10.1001/jama.2010.2008.
16. Wong DF, Moghekar AR, Rigamonti D, Brasic JR, Rousset O, Willis W, et al. An in vivo evaluation of cerebral cortical amyloid with [(18)F]Flutemetamol using positron emission tomography compared with parietal biopsy samples in living normal pressure hydrocephalus patients. Mol Imaging Biol. 2012. doi:10.1007/s11307-012-0583-x.
17. Maeda J, Ji B, Irie T, Tomiyama T, Maruyama M, Okauchi T, et al. Longitudinal, quantitative assessment of amyloid, neuroinflammation, and anti-amyloid treatment in a living mouse model of Alzheimer's disease enabled by positron emission tomography. J Neurosci. 2007;27:10957–68. doi:10.1523/JNEUROSCI.0673-07.2007.

18. Manook A, Yousefi BH, Willuweit A, Platzer S, Reder S, Voss A, et al. Small-animal PET imaging of amyloid-beta plaques with [11C]PiB and its multi-modal validation in an APP/PS1 mouse model of Alzheimer's disease. PLoS One. 2012;7:e31310. doi:10.1371/journal.pone.0031310.
19. Agdeppa ED, Kepe V, Liu J, Flores-Torres S, Satyamurthy N, Petric A, et al. Binding characteristics of radiofluorinated 6-dialkylamino-2-naphthylethylidene derivatives as positron emission tomography imaging probes for beta-amyloid plaques in Alzheimer's disease. J Neurosci. 2001;21:RC189.
20. Gallyas F. Silver staining of Alzheimer's neurofibrillary changes by means of physical development. Acta Morphol Acad Sci Hung. 1971;19:1–8.
21. Barghorn S, Davies P, Mandelkow E. Tau paired helical filaments from Alzheimer's disease brain and assembled in vitro are based on beta-structure in the core domain. Biochemistry. 2004;43:1694–703. doi:10.1021/bi0357006.
22. von Bergen M, Barghorn S, Muller SA, Pickhardt M, Biernat J, Mandelkow EM, et al. The core of tau-paired helical filaments studied by scanning transmission electron microscopy and limited proteolysis. Biochemistry. 2006;45:6446–57. doi:10.1021/bi052530j.
23. Fodero-Tavoletti MT, Mulligan RS, Okamura N, Furumoto S, Rowe CC, Kudo Y, et al. In vitro characterisation of BF227 binding to alpha-synuclein/Lewy bodies. Eur J Pharmacol. 2009;617:54–8. doi:10.1016/j.ejphar.2009.06.042.
24. Thompson PW, Ye L, Morgenstern JL, Sue L, Beach TG, Judd DJ, et al. Interaction of the amyloid imaging tracer FDDNP with hallmark Alzheimer's disease pathologies. J Neurochem. 2009;109:623–30. doi:10.1111/j.1471-4159.2009.05996.x.
25. Braak E, Braak H, Mandelkow EM. A sequence of cytoskeleton changes related to the formation of neurofibrillary tangles and neuropil threads. Acta Neuropathol. 1994;87:554–67.
26. Thal DR, Rub U, Schultz C, Sassin I, Ghebremedhin E, Del Tredici K, et al. Sequence of Abeta-protein deposition in the human medial temporal lobe. J Neuropathol Exp Neurol. 2000;59:733–48.
27. Villemagne VL, Furumoto S, Fodero-Tavoletti M, Harada R, Mulligan RS, Kudo Y, et al. The challenges of tau imaging. Future Neurol. 2012;7:409–21. doi:10.2217/fnl.12.34.
28. Fodero-Tavoletti MT, Smith DP, McLean CA, Adlard PA, Barnham KJ, Foster LE, et al. In vitro characterization of Pittsburgh compound-B binding to Lewy bodies. J Neurosci. 2007;27:10365–71. doi:10.1523/JNEUROSCI.0630-07.2007.
29. Klunk WE, Lopresti BJ, Ikonomovic MD, Lefterov IM, Koldamova RP, Abrahamson EE, et al. Binding of the positron emission tomography tracer Pittsburgh compound-B reflects the amount of amyloid-beta in Alzheimer's disease brain but not in transgenic mouse brain. J Neurosci. 2005;25:10598–606. doi:10.1523/JNEUROSCI.2990-05.2005.
30. Klunk WE, Wang Y, Huang GF, Debnath ML, Holt DP, Shao L, et al. The binding of 2-(4'-methylaminophenyl)benzothiazole to post-mortem brain homogenates is dominated by the amyloid component. J Neurosci. 2003;23:2086–92.
31. Shin J, Lee SY, Kim SH, Kim YB, Cho SJ. Multitracer PET imaging of amyloid plaques and neurofibrillary tangles in Alzheimer's disease. Neuroimage. 2008;43:236–44. doi:10.1016/j.neuroimage.2008.07.022.

Geriatrics Gerontology Medline Indexed

Geriatr Gerontol Int 2013; **13:** *215–221*

ORIGINAL ARTICLE: BIOLOGY

Brain accumulation of amyloid β protein visualized by positron emission tomography and BF-227 in Alzheimer's disease patients with or without diabetes mellitus

Naoki Tomita,[1] Katsutoshi Furukawa,[1] Nobuyuki Okamura,[3] Manabu Tashiro,[4] Kaori Une,[1] Shozo Furumoto,[3] Ren Iwata,[5] Kazuhiko Yanai,[3] Yukitsuka Kudo[2] and Hiroyuki Arai[1]

[1]Department of Geriatrics and Gerontology, Division of Brain Sciences, Institute of Development, Aging and Cancer, [2]Department of NeuroImaging Research, Innovation New Biomedical Engineering Center, Tohoku University, [3]Department of Pharmacology, Tohoku University Graduate School of Medicine, [4]Division of Cyclotron Nuclear Medicine, and [5]Division of Radiopharmaceutical Chemistry, Cyclotron and Radioisotope Center, Sendai, Miyagi, Japan

Aim: Although diabetes mellitus (DM) is considered to be one of the most consistent risks for developing dementia, it is not known if the pathology in dementia patients with DM is similar to or distinct from typical pathological features of Alzheimer's disease (AD). To discover the mechanism of developing dementia in AD patients with DM in a living state, we studied the distribution of amyloid β (Aβ) protein of diabetic AD patients.

Methods: To evaluate the accumulation of Aβ, we examined 14 normal controls, four diabetic patients with AD and 11 non-diabetic patients with AD by positron emission tomography (PET) using BF-227, a currently developed Aβ tracer.

Results: The analysis of PET images among the three groups showed an abundant aggregated Aβ accumulation in the cerebral cortex of both AD patients with and without DM. The extent and distributions of BF-227 accumulation in diabetic AD patients were not significantly different from these of non-diabetic AD patients.

Conclusion: These results suggest that the degree and extent of Aβ deposition is not significantly different between AD with DM and AD alone. **Geriatr Gerontol Int 2013; 13: 215–221.**

Keywords: Alzheimer's disease, amyloid β-peptides, diabetes mellitus, positron emission tomography.

Introduction

Long-standing lifestyle-related disorders from midlife, such as diabetes mellitus (DM) and hypertension, as well as obesity, are likely to be prominent risk factors for developing dementia and Alzheimer's disease (AD).[1] In fact, it is often found that diabetic patients develop AD in their later stage of life. Several separate community-based studies suggest that DM might increase the risk of dementia and AD,[2] though the underlying mechanisms are still not clearly explained.

Accepted for publication 9 April 2012.

Correspondence: Professor Hiroyuki Arai MD PhD, Department of Geriatrics and Gerontology, Division of Brain Sciences, Institute of Development, Aging and Cancer, Tohoku University, 4-1 Seiryomachi, Aobaku, Sendai 980-8498, Japan. Email: harai@idac.tohoku.ac.jp

AD is well characterized by an accumulation of misfolded proteins in the aging brain, which results in oxidative and inflammatory damage that in turn leads to energy failure and synaptic dysfunction.[3] In contrast, the impact of DM on the central nervous system (CNS) is not clearly understood.

Three major components related to type 2 DM that might underlie the effect of diabetes on the CNS in the development of AD are insulin resistance, hyperinsulinemia and hyperglycemia.[4] In addition to these three components, several other components are associated with the incidence of dementia or progression of cognitive decline. Whitmer *et al.* reported that severe hypoglycemic events were associated with a greater risk of dementia.[5] In addition, daily acute glucose fluctuations are also reported to be associated with cognitive decline.[6] Leptin, adiponectin and glucagon like peptide-1 (GLP-1) have recently been mentioned as potential factors that

doi: 10.1111/j.1447-0594.2012.00880.x

are associated with the development of AD.[7–10] These components are not fully independent of each other, and it is unlikely that the impact of DM on the CNS depends exclusively on a single component. Which components play the major role might depend on the patient's clinical history and the present state of DM.

Each of these components are thought to act on several different pathways that are important in the pathophysiology of AD, either indirectly, through inflammation or the development of vascular disease, or directly, through effects on amyloid and tau metabolism, and the formation of advanced glycation end-products (AGE).[11] (Fig. 1)

Autopsy results in an epidemiological study concluded that macroscopic brain infarcts are more common in people with DM than those without the disorder, as well as microvascular changes.[12] In contrast, the reported incidence of Alzheimer's pathology in the brains of people with diabetes varies between studies. There are several contradictory papers reporting the relationship between DM and AD. Beeri *et al.* have reported that type 2 DM is inversely associated with AD pathology; that is, diabetic patients with dementia have a significantly lower density of senile plaques than non-diabetic patients with dementia.[13] Matsuzaki *et al.* reported that hyperinsulinemia and hyperglycemia caused by insulin resistance are positively associated with the pathology of AD.[14] In the autopsy population of the Honolulu-Asia Aging Study, the occurrence of neurofibrillary tangles and amyloid plaques in the hippocampus and cortex in people without the apolipoprotein E (*APOE*) ε4 allele were similar to those with and without DM. However, as for *APOE* ε4 carriers, these lesions were more common in people with DM than in people without DM.[12] It was also reported that DM is related to generating atherosclerosis and cerebral infarction, but not directly to AD pathology in diabetic patients with dementia.[15,16] Autopsy findings are usually a mixture of many changes occurring during the living state, so the findings do not necessarily reflect the changes that are clinically relevant.

Interaction between medication for DM, especially the effect of insulin use, and AD neuropathology should be considered as well, as the population of insulin users showed a much higher risk of developing dementia in a cohort study.[17] Biessels *et al.* showed significantly fewer amyloid plaques in diabetic patients who received both insulin and oral antidiabetic medication, as compared with diabetic patients with other medication statuses or non-diabetic subjects. The effects of diabetes medication were specific to amyloid plaques, as the extent of neurofibrillary tangles pathology was not associated with diabetes medications.[18] However, these findings are derived from autopsies, and it is not certain if the same results can be gained from living human brains.

Several neuroimaging studies reported that DM is a risk factor for silent and symptomatic brain infarcts seen with magnetic resonance imaging (MRI),[19,20] and DM is also associated with cortical and subcortical atrophy.[21–23] As functional imaging, it is well known that reductions in regional cerebral glucose metabolic rate (CMRglu), as measured by fludeoxyglucose F 18 positron emission tomography (FDG-PET), are associated with increased AD risk and can be observed years before the onset of dementia.[24,25] Baker *et al.* reported that insulin resistance in persons with normal cognition and prediabetes or early diabetes without treatment is associated with reductions in CMRglu measured with FDG-PET.[26] However, previous radiological studies had limitations on discussing the pathological mechanism, as the modalities used were not directly linked to Alzheimer's pathology. No studies have been carried out regarding a pathobiological link between DM and AD in living human subjects.

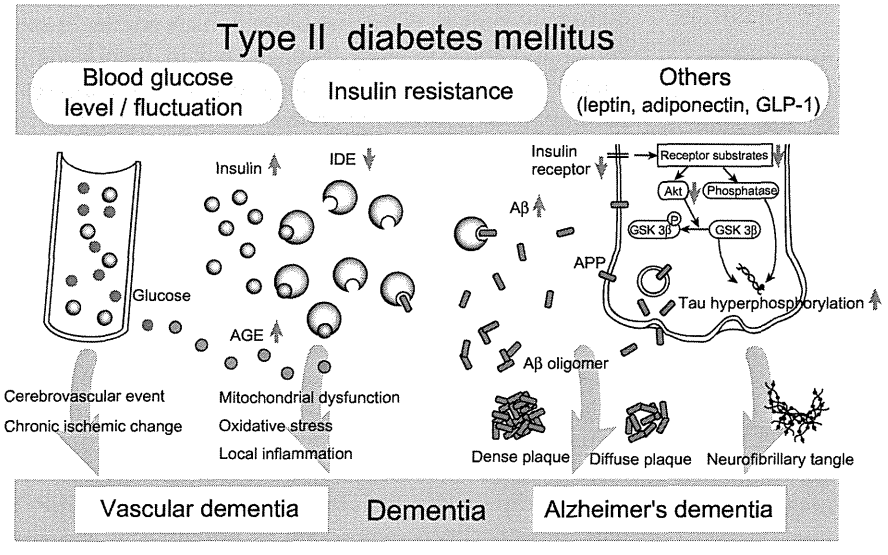

Figure 1 The possible pathological mechanisms associated with the impact of type 2 diabetes mellitus (DM) on the central nervous system (CNS). The major components of DM are described in the second column (only the three major components are described for easier understanding, though several other components are mentioned). Just below the column, the possible mechanism of developing dementia in type 2 DM. Aβ, amyloid β protein; AGE, advanced glycation end-products, APP, amyloid precursor protein; GLP-1, glucagon like peptide-1; GSK-3β, glycogen synthase kinase 3β; IDE, insulin degrading enzymes.